Proceedings of the 16th Czech and Slovak Conference on Magnetism, Košice, Slovakia, June 13–17, 2016

Differentiation of Native and Reconstructed Ferritin using the MRI Gradient Echo Pulse Sequence

L. Balejcikova[a,b,*], O. Strbak[a,c], L. Baciak[d], J. Kovac[b], M. Masarova[a], A. Krafcik[a], P. Kopcansky[b], D. Dobrota[c] and I. Frollo[a]

[a]Institute of Measurement Science, SAS, Dubravska cesta 9, 841 04 Bratislava 4, Slovakia
[b]Institute of Experimental Physics, SAS, Watsonova 47, 040 01 Kosice, Slovakia
[c]Biomedical Center Martin, Jessenius Faculty of Medicine in Martin, Comenius University in Bratislava, Mala Hora 4, 036 01 Martin, Slovakia
[d]Faculty of Chemical and Food Technology STU, Radlinskeho 9, 812 37 Bratislava, Slovakia

Ferritin is a biological iron storage biomacromolecule, consisting of a spherical protein shell (apoferritin) and mineral iron core. It plays a crucial role in the pathological processes of disrupted iron homeostasis followed by iron accumulation, linked with various disorders (e.g. neuroinflammation, neurodegeneration, cirrhosis, cancer, etc.) *In vitro* reconstructed ferritin, with the assistance of a non-invasive magnetic resonance imaging technique, has the potential to become a suitable biomarker of these pathological processes. Through gradient echo pulse sequencing, we were able to clearly distinguish between native (physiological) and reconstructed/iron-overloaded (pathological) ferritin, which can serve as a starting point for the development of a method for their differentiation. Such method is necessary for the early diagnosis of iron-based diseases.

DOI: 10.12693/APhysPolA.131.1093
PACS/topics: 75.60.Ej, 83.85.Fg, 87.61.–c, 87.64.Cc, 87.85.jf

1. Introduction

While the presence of iron in the human metabolism is essential [1, 2], excess iron ions is highly toxic for the organism [2]. Therefore, iron is stored in a non-toxic form of storage protein, ferritin, where it is kept as hydrous ferric oxide nanoparticles with a crystallographic structure similar to ferrihydrite mineral [3].

Ferritin consists of a hollow spheroid shell (apoferritin) 12 nm in diameter and formed by 24 subunits [4], with the total molecular weight ≈ 450 kDa [5]. Physiological ferritin has the potential to store up to 4500 iron atoms arranged in a crystal lattice [6, 7]. Iron is then released from ferritin according to the human body's specific requirements (pregnancy, homorrhage, iron deficiency diseases, etc.), regulated by an autocatalytic function of ferritin [3].

Disruption of the metabolism and the storage of iron in ferritin is closely related to cancer, neurodegenerative or cardiovascular diseases [8–10], involving the damage of ferritin and accumulation of iron ions [11]. Early diagnosis of these disorders can help in the correction of pathological processes and selection of an appropriate medical therapy to slow their progress. Magnetic resonance imaging (MRI) could represent such a diagnostic method, with its sensitivity to iron deposits detected through the modification of the MRI signal.

In the present work we studied native ferritin (NF) and reconstructed ferritin (RF) with different iron loadings as a pathological *in vitro* model system. Magnetisation of the samples was obtained using SQUID magnetometry up to 5 T, while colloidal stability was investigated utilising dynamic light scattering (DLS). MRI was employed to detect and discriminate the RF from NF, which could support applied research as a novel MRI contrast agent or standard for the diagnostics of various diseases associated with iron overload.

2. Experimental methods

NF, apoferritin and other chemicals were purchased from Sigma-Aldrich.

RF was prepared by the gradual addition (in 10 steps every 10 min) of ferrous ions (0.1 M solution of the Mohr salt) into the empty protein shell of apoferritin at 37 °C under constant stirring. The reaction solution with apoferritin (≈ 3 g/L) was added to 0.02 M HEPES buffer (pH 7.4), previously deaerated using inert nitrogen over 1 h to provide anaerobic conditions and controlled oxidation of ferrous ions via a 0.07 M solution of trimethylamine N-oxide. Several samples of RF with different loading factors (LFs), representing the average number of iron atoms per one apoferritin biomacromolecule, were prepared.

Quantitative analysis of the LF was conducted utilising a UV-VIS spectrophotometer SPECORD 40 (Analytik Jena) at 25 °C via a previously-reported process [12].

The average hydrodynamic diameter $\langle D_{HYDR} \rangle$ of the studied objects in aqueous solution was measured by Zetasizer NanoZS 3600 (Malvern Instruments) at 25 °C, employing the DLS method in disposable polystyrene cuvettes in the protein data analysis mode.

*corresponding author; e-mail: balejcikova@saske.sk

The magnetic properties of the nanoparticles inside the proteins were studied using a SQUID magnetometer (Quantum Design MPMS 5XL) with induction of the magnetic field up to 5 T.

Relative contrast measurements were performed at 0.2 T ESAOTE and 4.7 T VARIAN systems for comparison. In the low-field system, standard T_2-weighted pulse sequences were used: the gradient echo (GE) protocol with repetition time $TR = 600$ ms and echo time $TE = 22$ ms; the short-T_1 inversion recovery (STIR) protocol with $TR = 1960$ ms and $TE = 80$–120 ms; and the turbo spin echo (TSE) protocol with $TR = 3000$ ms and $TE = 80$–120 ms. In the high-field system the images were acquired with T_2-weighted multi-echo-multi-slice (MEMS) sequence, with $TR = 81$ ms and $TE = 8$ ms. The transverse relaxation time T_2 was obtained spectroscopically via the Car–Purcell–Meiboom–Gill (CPMG) echo pulse sequence.

The relative contrast is defined as follows:

$$RC = (I - I_0)/I_0, \tag{1}$$

where I_0 is the signal intensity without magnetite nanoparticles, and I represents the signal intensity with magnetite nanoparticles. The transverse relaxivity R_2 is calculated as follows:

$$R_2 = r_2 C + R_2^0, \tag{2}$$

where R_2^0 is the transverse relaxation rate in the absence of nanoparticles, r_2 represents the transverse relaxation rate in the presence of nanoparticles, and C is the nanoparticles' concentration.

For image data processing and basic analysis we used the following software tools: Marevisi (NRC — Institute for Biodiagnostics, Winnipeg, Canada), and Matlab R2011b (Mathworks Inc., Natick, USA).

3. Results and discussion

The modifications of the *in vitro* chemicals' synthesis conditions enabled the preparation of RF with various LFs, determined spectrophotometrically with less than 2% error (Table I). NF was diluted in 0.02 M HEPES buffer (pH 7.4) to obtain ≈ 3 g/L concentration, for comparison with the RF samples.

Table I shows the average $\langle D_{HYDR} \rangle$ of the hydrated/solvated protein biomacromolecules in aqueous solutions changed according to the LF, while the polydispersity indexes (PDIs) underscore the polydispersity growth as a function of the LF. A PDI with a maximum value of 1.000 indicates strong aggregation of the RFs, most likely caused by the iron binding and overload effect.

The magnetic properties of the RFs were compared with NF. The magnetisation-field dependences of all samples did not show hysteresis at 295 K, which is typical for the superparamagnetic behaviour of small nanoparticles. None of the samples presented with saturation magnetisation, which could be associated with ferrihydrite-like iron core. Magnetisation depends on the LF (Fig. 1), which could be related to the various sizes of the RFs or aggregation (Table I).

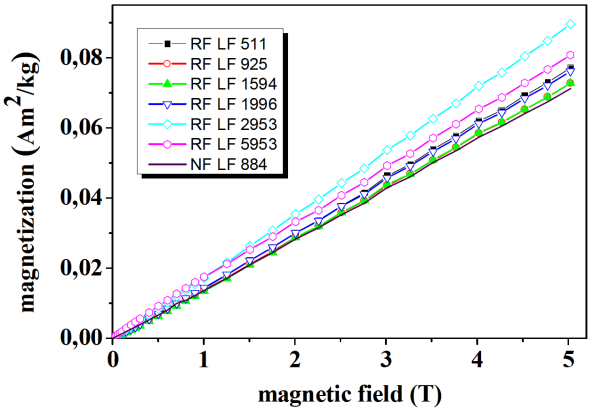

Fig. 1. Magnetisation curves of RF in comparison with NF measured at 290 K.

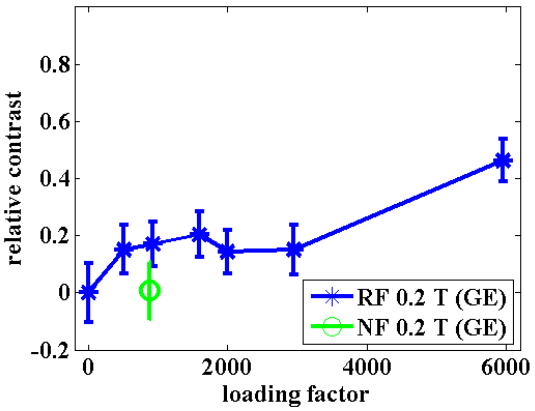

Fig. 2. The relative contrast of RF and NF with different LFs measured at 0.2 T with GE pulse sequence ($TR = 600$ ms, $TE = 22$ ms).

Figure 2 presents the relative contrast of RF and NF measured at 0.2 T with GE pulse sequence, in comparison with different LFs. It is possible to clearly distinguish between the RF and NF; however, we only observed such a difference (almost 20%) with the GE protocol. One possible explanation is that the STIR and TSE protocols are less sensitive to the field inhomogeneities produced by the reconstructed iron core of apoferritin, which can have a different magnetic phase and magnetic moment,

TABLE I

Basic parameters obtained from UV-VIS quantitative analysis and DLS measurements.

Sample	LF	$\langle D_{HYDR} \rangle$ [nm]	PDI
NF	884	17.27	0.437
RF	511	19.05	0.276
RF	925	31.88	0.461
RF	1594	284.50	0.747
RF	1996	364.80	0.795
RF	2953	192.30	1.000
RF	5953	91.11	1.000

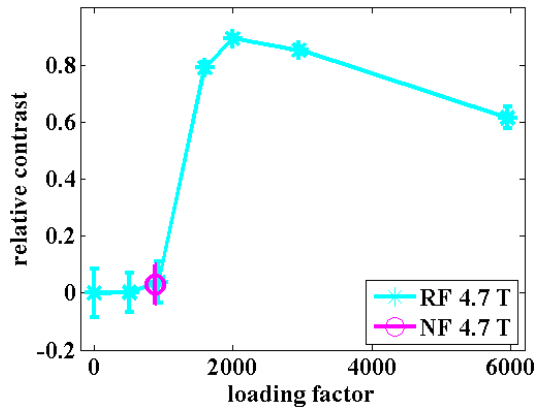

Fig. 3. The relative contrast of RF and NF with different LFs, measured at 4.7 T with spin echo pulse sequence ($TR = 81$ ms, $TE = 8$ ms).

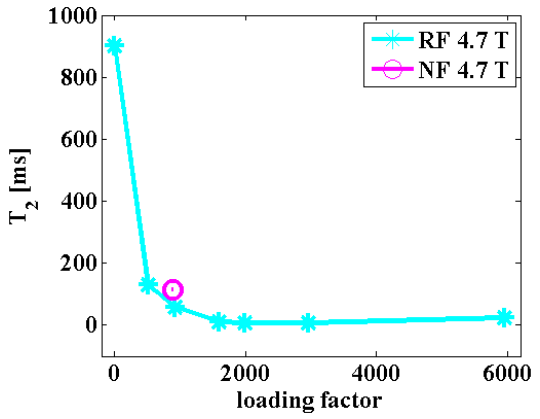

Fig. 4. The transversal relaxation time T_2 of RF and NF obtained spectroscopically through the CPMG echo pulse sequence at 4.7 T.

in comparison with NF. On the other hand, we utilised only standard clinically-used T_2-weighted protocols with different echo times. In the case of optimisation procedures, it is highly possible that we would also be able to differentiate native and RF with other protocols.

Regarding the high-field relative contrast measurements we see a slightly modified trend, as in the low-field STIR and TSE protocols. Here, it is not possible to distinguish the NF from the RF (Fig. 3). Virtually the same situation is also found with the transversal relaxation time T_2 comparison (Fig. 4). Relaxation of protons in higher magnetic fields evidently suppresses the subtle shifts in the magnetic phase of the mineral core of the RF, which causes the difference in the relative contrast of the GE pulse sequence.

4. Conclusions

Our results provide comparative study of RF with different LFs and NF through a combination of DLS, SQUID magnetometry and MRI measurement. The DLS data revealed increased average hydrodynamic diameter and polydispersity with LF growth. Magnetisation data were used to distinguish the various superparamagnetic RFs. Differences in MRI contrast in the GE pulse sequence could allow discrimination between RF and NF, which may prove useful in the diagnosis of non-invasive disorders (e.g. neurodegenerative diseases) associated with iron accumulation and overloading. We have demonstrated that MRI has the potential to become a simple and fast method that is sufficiently sensitive for the imaging of iron-related pathological tissues.

Acknowledgments

This work was supported through the Slovak Research and Development Agency, project no. APVV-0431-12, APVV-15-0029 and the Slovak Scientific Grant Agency, project VEGA nos. 2/0013/14 and 1/0377/16.

References

[1] C.W. Connie, M.D. Hsia, *N. Engl. J. Med.* **338**, 239 (1998).

[2] D. Finazzi, P. Arosio, *Arch. Toxicol.* **88**, 1787 (2014).

[3] N.D. Chasteen, P.M. Harrison, *J. Struct. Biol.* **126**, 182 (1999).

[4] E.C. Theil, H. Takagi, G.W. Small, L. He, A.R. Tipton, D. Danger, *Inorg. Chim. Acta* **297**, 242 (2000).

[5] M. Wagstaff, M. Worwood, A. Jacobs, *Biochem. J.* **173**, 969 (1978).

[6] Y. Ren, T. Walczyk, *Metallomics* **6**, 1709 (2014).

[7] Y.-H. Pan, K. Sader, J.J. Powell, A. Bleloch, M. Gass, J. Trinick, A. Warley, A. Li, R. Brydson, A. Brown, *J. Struct. Biol.* **166**, 22 (2009).

[8] A. Friedman, P. Arosio, D. Finazzi, D. Koziorowski, J. Galazka-Friedman, *Parkinsonism Relat. Disord.* **17**, 423 (2011).

[9] M.J. Williams, R. Poulton, S. Williams, *Atherosclerosis* **165**, 179 (2002).

[10] A.A. Alkhateeb, J.R. Connor, *Biochim. Biophys. Acta* **1836**, 245 (2013).

[11] P. Nielsen, U. Günther, M. Dürken, R. Fischer, J. Düllmann, *J. Lab. Clin. Med.* **135**, 413 (2000).

[12] Z. Mitróová, L. Melníková, J. Kováč, M. Timko, P. Kopčanský, *Acta Phys. Pol. A* **121**, 1318 (2012).